

Hydrodynamics of model *Posidonia oceanica* patches in shallow water

Andrew M. Folkard¹

Department of Geography, University of Lancaster, Lancaster LA1 4YB, United Kingdom

Abstract

The hydrodynamics of simulated patches of the Mediterranean seagrass *Posidonia oceanica* were studied in laboratory flume experiments in which the height of the pruned canopy was always greater than half the total water depth. The effects of variations in speed (from 0.08 m s⁻¹ to 0.24 m s⁻¹) and patch configuration on the hydrodynamics were investigated. Significant speeds penetrated the patches to approximately half their height. Reducing speed did not change the flow patterns observed, except to weaken and blur them. Flow encountering a single patch formed a turbulent wake at the height of the top of the canopy. Within this wake, the vertical shear stress decreased monotonically downstream, but the Reynolds stress increased initially and then decayed. When a second patch was positioned within the region where Reynolds stress increased (referred to as the “06 patch”), the wake center penetrated it, causing average turbulent velocities with horizontal components 3.3 times higher and vertical components 4.2 times higher than in the upstream patch. When this patch was positioned where the Reynolds stress decayed (referred to as the “14 patch”), the wake center rose above it. Nevertheless, the turbulence in the 14 patch had horizontal components 12% higher and vertical components 22% higher on average than in the 06 patch because its upstream end was closer to the Reynolds stress maximum. Thus the ratio of the patch separation to the length of wake in which the Reynolds stress increased was identified as central to quantifying the turbulence within the downstream patch. The increased turbulence is likely to be important in determining sedimentary and ecological patch characteristics by increasing retention of particulates in suspension and thus reducing depositional rates of, for example, larvae, nutrients, and dead organic matter.

The interaction of flows with seagrass meadows affects many ecological processes such as the transport and interception of pollen by seagrass carpels (e.g., Ackerman 2002), the supply of dissolved nutrients to seagrass leaves (e.g., Cornelisen and Thomas 2004), and sediment nutrient dynamics (Rose and Dawes 1999). Abdelrhman (2003) has provided a mathematical model of many of these effects. Patchiness of seagrass meadows alters the nature of this interaction. The degree of patchiness is positively correlated with current velocity (Fonseca et al. 1983)—possibly because flow acceleration around patches causes local erosion, thus sustaining their isolation (Gambi et al. 1990)—and the spatial distribution of patches profoundly affects the flow field around them (Granata et al. 2001). Patch size and distribution are also important in determining the distribution of seagrass-associated fauna (e.g., Irlandi 1997; Bologna and Heck 2002; Tanner 2003). Flow conditions are important determinants of the meadow-scale morphodynamics of fragmented seagrass communities (Fonseca and Bell 1998). Recognition of this has informed predictive mapping strategies

used to aid restoration and conservation of seagrass meadows (e.g., Kelly et al. 2001).

Patchiness also affects rates of sedimentary deposition and resuspension via a complex set of interactions between patch distribution, flow dynamics, balances of organic and mineral sediments, suspended particulate chemistry, and edaphic development (e.g., Madsen et al. 2001; Gacia et al. 2003). Sedimentary processes in turn determine turbidity around seagrass patches and thus the supply of light to them (e.g., Dennison and Alberte 1985).

Finally, seagrass patchiness affects hydraulics and consequently macroscale (e.g., whole estuary) suspended particulate matter budgets. This effect is generally quantified through drag coefficients, which may be functions of plant size, morphology, and density, and flow depth and speed. Fragmentation of seagrass meadows can significantly alter circulation patterns (Fonseca and Fisher 1986). Because of complex interactions between waves, currents, and tides in seagrass meadows, their frictional drag cannot be characterized by single-parameter equations, even when they are homogeneous (Teeter et al. 2001). The only feasible approach to this problem, and the one used herein, is to analyze small-scale processes (e.g., Abdelrhman 2003) and infer from these the macroscale implications.

The present research furthers understanding of this issue by reporting detailed flume investigations of flow in and around simulated patches of *Posidonia oceanica*, a seagrass common throughout the Mediterranean Sea. This is novel in that *P. oceanica* has a different morphology from that of aquatic macrophytes previously studied in flume experiments (e.g., Fonseca et al. 1982; Nepf et al. 1997; Nepf and Vivoni 2000) and understanding of the hydrodynamics of patchy seagrass beds is currently lacking. The specific objectives of our study are firstly, to identify and quantify the patterns of mean flow and turbulence found in the vicinity

¹ Corresponding author (a.folkard@lancaster.ac.uk).

Acknowledgments

Discussions with Giuseppe Ciruolo, Antonino Maltese, Gofredo La Loggia, Giovanni Ferrerri, Sebastiano Calvo, Eleanor Cox, and Alastair Kirkbride significantly contributed to the interpretation of the data. The comments of Joe Ackerman, Mark Fonseca, and one anonymous referee at the review stage significantly improved the quality of the paper. Dora Ferrerri constructed the seagrass simulations. Ian Thomas carried out some of the preliminary experiments. Charles Blakeley provided technical assistance. Funding from the British Council/Italian MURST UK-Italian Exchange Program allowed the collaboration that led to this work to be initiated. To all these, the author expresses his gratitude.

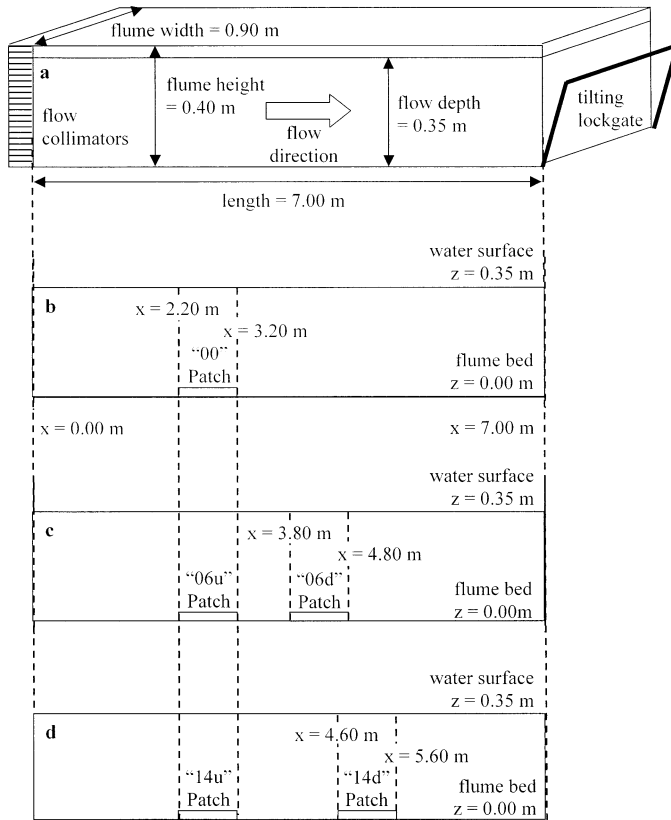


Fig. 1. Schematic diagram (a) of the experimental flume and positions (b–d) of the seagrass patch bases in (b) “00” cases, (c) “06” cases, and (d) “14” cases.

of the simulated *P. oceanica* patches in shallow conditions; secondly, to determine how these structures affect the hydrodynamic environment within the patches; and thirdly to determine the ecological, sedimentary, and hydraulic implications of the hydrodynamics observed.

Methodology

The research was carried out in a recirculating laboratory flume (Armfield) with an experimental section 7.00 m long, 0.90 m wide, and 0.40 m high (Fig. 1). A beehive arrangement of flow collimators at the inlet strongly damped discrepancies from uniform downstream flow due to entrance conditions. Individual sections of simulated seagrass, each 1 m long, were attached to the otherwise flat, horizontal bed of the flume to represent isolated patches of *P. oceanica*. The patch bases were constructed from plywood. The simulated seagrass plants were located by dividing the base into squares with sides 36.5 mm long. A 5-mm diameter hole was then drilled into the base at a random position in each of these squares (assigned by the random number generator within a Microsoft Excel spreadsheet), and the simulated seagrass plants were placed in these holes. This produced a plant density of $\sim 750 \text{ m}^{-2}$, which represented densities of *P. oceanica* found in nature (e.g., Mazzella et al. 1995) while avoiding straight lines and thus preferential flow paths through the patch.

The seagrass plants were simulated using polyethylene sheeting (Decco) whose thickness, $\sim 0.2 \text{ mm}$, was the same as the mean thickness of several sample leaves of *P. oceanica* collected manually during the peak of the growing season (July) from the Sicilian coastline. The plastic sheeting had density $\rho = 900 \pm 20 \text{ kg m}^{-3}$ (this and all following values quoted as mean $\pm 1 \text{ SD}$, sample size $n = 10$), modulus of elasticity $E = 5.4 \pm 0.1 \times 10^8 \text{ N m}^{-2}$ (determined by measuring the angle of deflection of a small cantilevered strip of the sheeting when loaded with small weights), and coefficient of kinetic friction $\mu = 0.47 \pm 0.03$ (when dry, using a small copper weight to test the angle of inclination of the sheeting at which motion was initiated against friction). These may be compared to average values measured in the same way for natural *P. oceanica* of $\rho = 910 \pm 110 \text{ kg m}^{-3}$, $E = 4.7 \pm 0.6 \times 10^8 \text{ N m}^{-2}$, and $\mu = 0.44 \pm 0.04$, respectively. The elastic modulus values are approximately coincident with the upper limit of the range $5.0 \times 10^5 \text{ N m}^{-2}$ to $3.7 \times 10^8 \text{ N m}^{-2}$ found by tensometer measurements of reproductive shoots of *Zostera marina* by Patterson et al. (2001). ρ and E will determine the pronation of the canopy and the nature of its oscillatory motion in response to the flow, and μ will determine in part the nature of flow attenuation and turbulence production within the canopy. The similarity of these values provides support for the use of the physical model to simulate natural plants.

Each simulated plant consisted of three pairs of leaves. Based on measurements of mature *P. oceanica* found in nature, these were cut to a width of 1 cm and lengths of 0.50 m, 0.25 m, and 0.15 m, respectively. The leaves were arranged with the shortest ones innermost and the longest outermost. Each plant was secured in its hole with silicone sealant. When a flow was passed over this arrangement, it produced a dense, partially pronated canopy with a three-layer structure. In the lowest, densest layer, from its base up to 30% of its height, all three pairs of leaves were present. In the middle layer, between 30% and 50% of its height, the two longer pairs of leaves were present. In the upper layer, which formed the upper half of the canopy, only the longest pair of leaves was present.

The boards were secured in the tank such that their bases were raised approximately 4 cm above the channel bed. This was considered appropriate in that it simulated the tendency for *P. oceanica* patches to grow on mounds of organic debris known as “matte” (e.g., Mateo et al. 1997). Although the square-cornered lip of the stand base used here is very different from the smooth mounds on which seagrass patches typically grow, no significant effect of this difference was observed, perhaps because the dense canopy immediately downstream damped any turbulence formed.

The hydrodynamic effect of a seagrass patch depends on the density of its foliage. This is quantified as the foliage area density $a(z)$ (Kaimal and Finnigan 1994). The high plant density used meant it was not possible to measure $a(z)$ precisely because this required measurement of the orientation of every leaf and the degree of overlap between leaves. However, upper limits $a(z)_{\text{max}}$ could be calculated by assuming each leaf was providing maximum obstruction to the flow—i.e., every leaf was oriented with its width perpendicular to the flow and there was no hiding of leaves by others

due to overlapping when viewed from upstream. In the upper half of the canopy, $a(z)_{\max} = 15 \text{ m}^{-1}$. Between 30% and 50% of the canopy height, $a(z)_{\max} = 30 \text{ m}^{-1}$, and in the lower 30% of the canopy, $a(z)_{\max} = 45 \text{ m}^{-1}$. These values are much higher than those of similar plant simulations used by, for example, Nepf and Vivoni (2000) in which $a(z) < 6 \text{ m}^{-1}$. In practice, the lower half of the canopy formed an almost impenetrable mass of leaves, suggesting very limited flows in this region. In fact, the high plant density made velocity measurements in this part of the canopy impossible.

Flow speed and depth were controlled by a variable speed pump and a tilting gate at the downstream end of the channel (Fig. 1). Depth was held constant in all runs at 0.35 m at the center of the flume, this being 70% of the longest leaf length, thus representing a typical shallow-water environment. Note, however, that the leaves remained submerged throughout the experiments because they were pronated by the flow. Little variation in depth ($< 5 \text{ mm}$) was observed over the length of the flume. Three discharge rates were used: 25, 50, and 75 L s^{-1} . These gave average speeds of 0.08 m s^{-1} (representing peak tidal flow; e.g., Gacia et al. 1999), 0.16 m s^{-1} , and 0.24 m s^{-1} (representing storm conditions, e.g.; Granata et al. 2001), respectively. Since the plants were simulated at full scale, no dynamical scaling of the experimental results was required. The Froude numbers for each of these discharge rates were, upstream of the patches, 0.043, 0.086, and 0.130, respectively. Where a portion of the flow passed rapidly over the patches, local Froude numbers rose to 0.14, 0.23, and 0.47, respectively (using the mean depth of the velocity profile inflection point as the depth scale). Thus the flow was subcritical in all cases, and no transitions of flow criticality occurred.

Three configurations of seagrass patches were used. In the first, a single patch was placed 2.20 m from the inflow; this was found sufficient in preliminary experiments to allow near-uniform downstream flow to be established prior to meeting the patch. Any nonuniformities were in any case swamped by the effect on the flow patterns of the patch itself. In the second and third configurations, a second patch was placed downstream. Preliminary measurements of the single patch wake showed distinct “near wake” and “far wake” regions. These are defined below. The downstream patch was placed such that its upstream end was in the near wake (0.6 m from the upstream patch) in the second configuration, and in the far wake (1.4 m from the upstream patch) in the third (see Fig. 1).

The three discharge values used are referred to as “fast” (75 L s^{-1} , average speed 0.24 m s^{-1}), “medium” (50 L s^{-1} , 0.16 m s^{-1}), and “slow” (25 L s^{-1} , 0.08 m s^{-1}). The three patch configurations are denoted “00” (single patch), “06” (0.60-m gap between patches), and “14” (1.40-m gap). Thus, for example, m06 is the case where the discharge is 50 L s^{-1} and there is a 0.60-m gap between the patches. In the 06 and 14 cases, the suffixes “u” and “d” denote the upstream and downstream patches, respectively. Thus, for example, the m06u patch is the upstream patch in the m06 case. U, V, and W denote the downstream, cross-stream, and vertical components of the mean flow, and u' , v' , and w' the values of the respective turbulent fluctuations. The latter trip-

let of symbols with overbars denotes their root mean square values over the whole time series from each location.

For each of the nine combinations of discharge values and patch configurations, time series of the downstream, transverse, and vertical components of velocity were measured using an Acoustic Doppler Velocimeter (Model NDV, Nortek) at a series of points. Vertical positions of these points (z) were measured upwards from the bed. Horizontal positions (x) were measured downstream from the upstream end of the tank. All measurements were taken in the central x - z plane. The measurement grid had a longitudinal separation of 20 cm, from $x = 1.00$ –6.00 m, and a vertical separation of 2 cm, from $z = 0$ –30 cm. Because there is 5 cm between the ADV and its sampling volume, the top 5 cm of the flow could not be measured directly and had to be extrapolated. The ADV was positioned on a trolley mounted on runners on either side of the flume that facilitated accurate vertical and horizontal location. The ADV software provided measurements of the sample volume height above the bed which acted as a check on the positioning measured by a Vernier scale on the trolley. Measurements at each position were taken for 120 s at 25 Hz. Details of ADV operation and calibration provided by Lane et al. (1998) were followed.

Problems were encountered in obtaining good time series within the canopy where leaves interfered with the operation of the ADV. Since the data obtained when leaves altered the signal from the ADV differed qualitatively from that when they did not, rejection of bad time series during experimentation was carried out subjectively, and repeat attempts to take data were made from the same location. Obtaining a good signal from the lower 50% of the canopy (where $a(z)_{\max} \geq 30 \text{ m}^{-1}$) proved impossible. As a result, only data from within the top half of each canopy are presented here.

The raw data were processed, following Lane et al. (1998), by applying a threshold of $> 70\%$ to the signal-correlation time series and low-pass filtering to remove high-frequency Doppler noise. In most time series, at least 95% of data points were retained, although in some this fraction was considerably lower.

In all of the runs carried out, the resulting data set consisted of a grid of data with some nodes missing, either because it had been impossible to obtain good data from them, or because the data obtained had been filtered out during processing. As a result, Surfer software (Golden Software) was used to interpolate, via kriging, the data onto a standard grid, with a node every 7 cm longitudinally and 1 cm vertically (note that this is considerably higher resolution than that at which the measurements were made). Within this grid, regions representing the impermeable bases of the patches and the nonmeasurable parts of the canopies are blanked out.

Results

Figure 2 shows plots of (U, W) for the fast-flow cases using data from the patches and the gap only. The seagrass became increasingly pronate as the discharge increased: In the slow-flow case, the top of the canopy was at $z \sim 30 \text{ cm}$, compared to $z \sim 22 \text{ cm}$ and $z \sim 17.5 \text{ cm}$ in the medium-

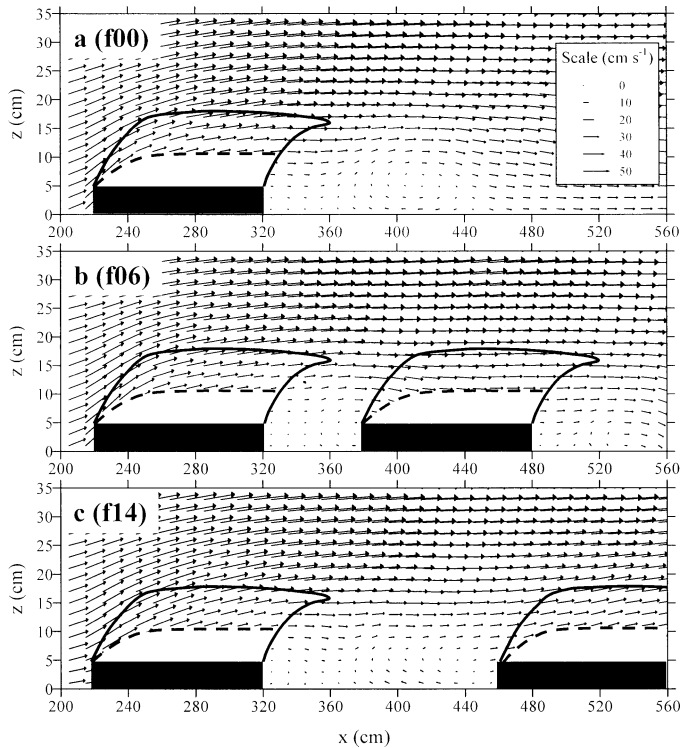


Fig. 2. Vector plots of the mean flow fields for (a) the f00 case, (b) the f06 case, and (c) the f14 case. The black sections indicate the patch bases, the clear white sections the nonmeasurable parts of the patches, the black dashed lines delineate the measurable and nonmeasurable parts of the patch, and the thick black outlines the extent of the patch canopies. The scale in (a) is that used for all three figures. These vectors have been interpolated from raw data (see text) and are shown at lower resolution than the fully interpolated data set for clarity.

and fast-flow cases, respectively. All three, however, took on similar morphologies. At the upstream end, the canopy rose rapidly to its maximum height, which was maintained to the end of the patch base. Beyond this, an overhanging region of increasingly sparse leaves extended to ~ 40 cm downstream of the base. Within the overhang, the leaves flapped with greater amplitude (~ 1 cm) than in the canopy body, where movements were of the order of a few millimeters. All these values were measured separately and not derived from the data in Fig. 2.

In the f00 case (Fig. 2a) the flow, on encountering the seagrass patch, separated into a rapid overflow and an attenuated flow through the patch. Immediately downstream of the tip of the seagrass, the shear layer thus formed at the top of the canopy separated and formed a recirculation cell centered at $x \sim 4.10$ m. Beyond this, largely downstream flow reformed. There was no recirculation cell in either the f06 or f14 cases (Fig. 2b,c). Instead, weak upwelling was observed. Otherwise, the mean flow was similar to the f00 case, except that the downstream patches maintained the shear flow whereas it decayed in their absence. The medium- and slow-flow cases show similar, less-coherent versions of the equivalent fast flow (U, W) fields (data not presented).

Figure 3 shows the Reynolds stress $-\overline{u'w'}$ for the fast-

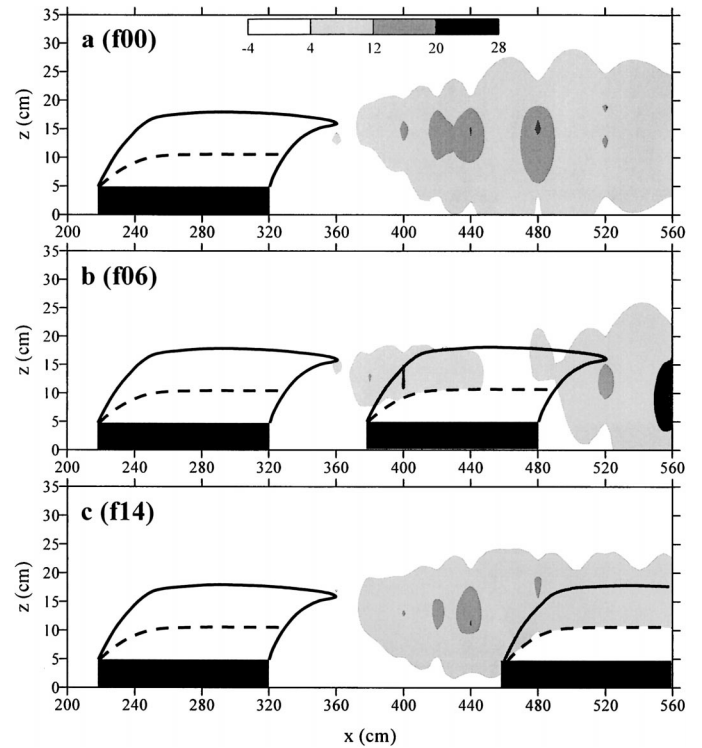


Fig. 3. Distribution of the Reynolds stress $-\overline{u'w'}$ for (a) the f00 case, (b) the f06 case, and (c) the f14 case. Canopies are represented as in Fig. 2. Contours in this and subsequent figures have been derived from interpolation of the raw data (see text) and smoothed via a constrained spline algorithm. The scale in (a) applies to all three figures and is in $\text{cm}^2 \text{s}^{-2}$.

flow cases. This provides a measure of the net vertical flux of downstream momentum due to turbulence. The f00 case (Fig. 3a) shows a wake with strongly positive $-\overline{u'w'}$ emanating from the downstream end of the seagrass and centered at $z \sim 15$ cm. In the f06 and f14 cases (Fig. 3b,c), the wake is similar to the f00 case, but in the former it is weakened by interaction with the f06d patch. In comparison to the f00 case, the m00 and s00 cases (Fig. 4a,b) show a similar but much weaker wake pattern. In the m00 case, the wake rises to the surface, rather than remaining approximately horizontal as the f00 wake does.

Other measures of turbulent activity, such as the vertical turbulent kinetic energy (TKE) $\overline{w'^2}$ and the horizontal TKE $(\overline{u'^2} + \overline{v'^2})$ show similar spatial patterns to $-\overline{u'w'}$. However, the locus of the $(\overline{u'^2} + \overline{v'^2})$ maximum descends more than that of either $\overline{w'^2}$ or $-\overline{u'w'}$ (Fig. 5), implying that most of the vertical momentum exchange in the wake occurs on its upper side.

Figure 6 shows the positions and values of the vertical profile maxima of $-\overline{u'w'}$. These plots have been smoothed using a five-point rolling mean in order to show more clearly the trends in variation. At the downstream end of the canopy in the f00 case (Fig. 6a), the $-\overline{u'w'}$ maximum is near the top of the canopy ($z \sim 15$ cm). It remains at this height thereafter (cf. Fig. 3a). Downstream, the $-\overline{u'w'}$ maximum value increases sharply as far as $x \sim 4.35$ m, and it decreases thereafter. This peak occurs above the downstream edge of

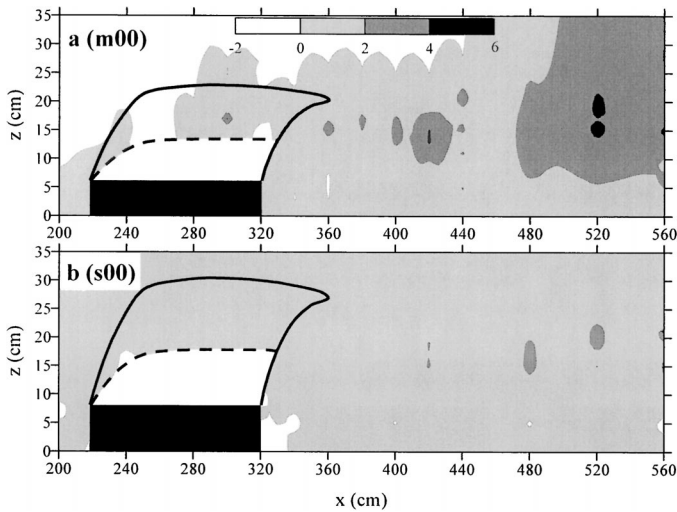


Fig. 4. Distribution of the Reynolds stress $-\overline{u'w'}$ for (a) the m00 case, and (b) the s00 case. Canopies are represented as in Fig. 2. Contours have been smoothed as in Fig. 3. The scale in (a) applies to both figures and is in $\text{cm}^2 \text{s}^{-2}$.

the recirculation cell. There is thus a qualitative change in both the mean and turbulent flow at this point. Therefore, it is taken to represent the boundary between the “near wake” (increasing vertical exchange of momentum in the wake, recirculating mean flow cell) and the “far wake” (decaying turbulent wake, increasingly uniform mean flow). The length of the near-wake region in this case is $L_{NW} \sim 1.20 \text{ m}$. Figure 7 shows plots of $-\overline{u'w'}$ maximum values for the three single-patch cases. L_{NW} increases with canopy height; indeed the data for the s00 case do not peak before the downstream end of the flume.

The $-\overline{u'w'}$ maxima in the f06 case (Fig. 6b) increase sharply at the downstream end of the f06u canopy, similarly to the f00 case. However, they then decrease sharply within the f06d canopy. From the downstream end of the f06u patch the positions of these maxima remain, as in the f00 case, at $z \sim 15 \text{ cm}$. Thus the wake of the f06u canopy partially penetrates the f06d canopy, which reduces $-\overline{u'w'}$ within the wake. In the f14 case (Fig. 6c), the $-\overline{u'w'}$ maxima show a very similar pattern to that in the f00 case. The positions of the maxima within the vertical profiles are also very similar, except for a slight rise over the f14d canopy, in contrast to the f06 case.

Figure 8 shows the same plots for the vertical shear stress $\partial U/\partial z$, again smoothed using a five-point rolling mean. Figure 8a shows that, in the f00 patch, the $\partial U/\partial z$ maximum lies within the canopy and increases in value downstream, reaching their global maximum at the end of the canopy. They then decrease monotonically beyond the canopy. The difference in the downstream locations of the global maxima of $-\overline{u'w'}$ and $\partial U/\partial z$ implies that up to the end of the near wake, the rate at which turbulence is produced by the shear stress is greater than that at which it is dissipated by Reynolds stresses. As the shear stress decays in the absence of the canopy, the turbulent production rate decreases until it is less than the dissipation rate. Thus the global maximum of

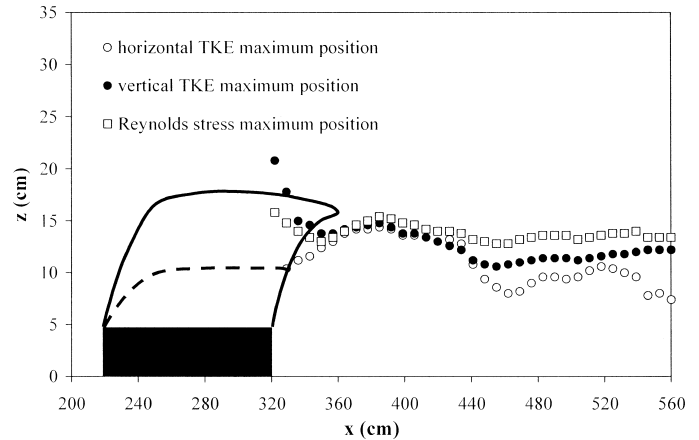


Fig. 5. Loci of the vertical profile maxima of Reynolds stress, horizontal, and vertical TKE for the f00 case.

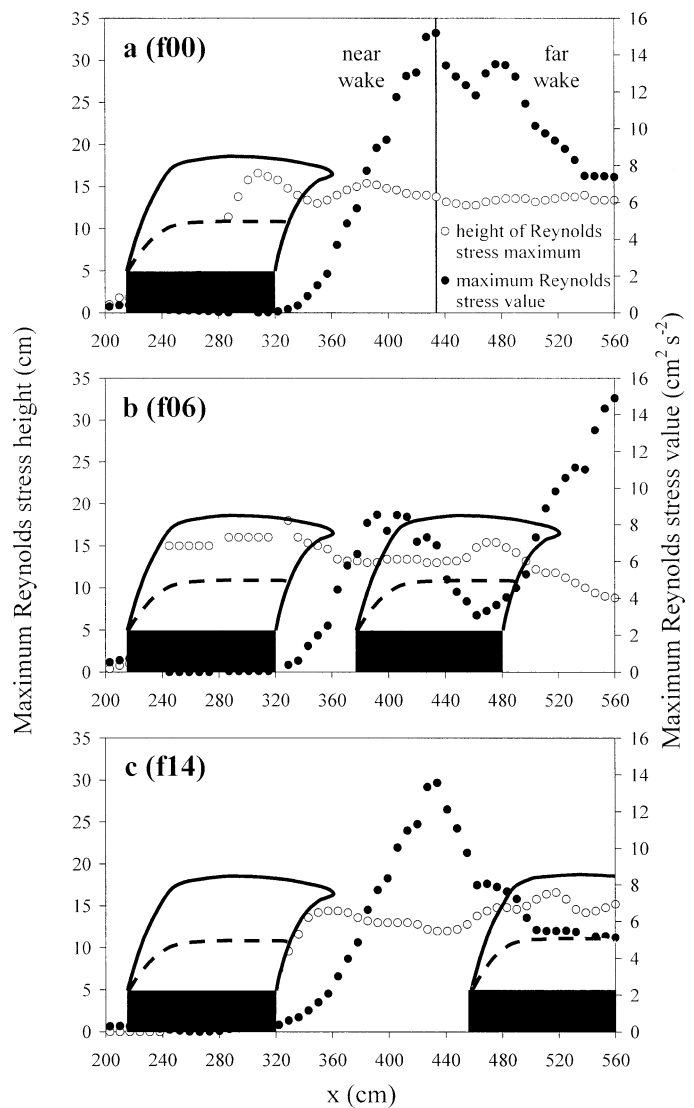


Fig. 6. Positions and values of the local vertical profile maxima of the Reynolds stress for (a) the f00 case; (b) the f06 case; (c) the f14 case. Data have been smoothed using a five-point rolling mean.

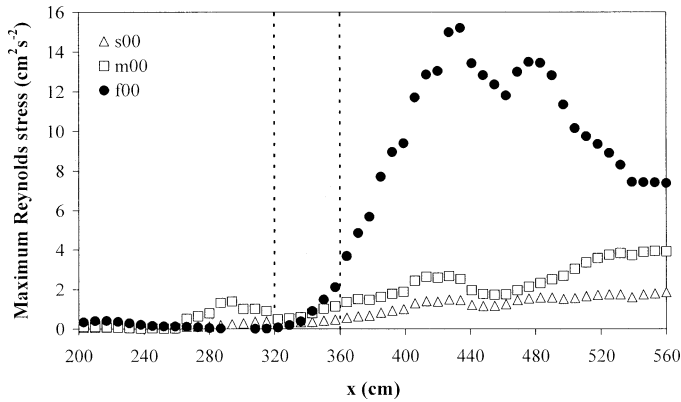


Fig. 7. Values of the local vertical profile maximum Reynolds stress for the three single-patch cases. The left-hand dotted line indicates the position of the downstream end of the patch base; the right-hand line indicates the end of the canopy overhang. Data have been smoothed using a five-point rolling mean.

$-\overline{u'w'}$ represents the point at which the production of turbulence in the wake ceases to exceed its dissipation.

The $\partial U/\partial z$ plots for the f06 and f14 cases (Fig. 8b,c) show similar patterns to the f00 case in terms of both the values and positions of the local maxima. However, there is a clear difference in the action of the f06d and f14d patches on the vertical profile of $\partial U/\partial z$. The $\partial U/\partial z$ maximum remains at approximately the half height of the f06d canopy throughout its length, but rises to the top of the f14d canopy about halfway along it.

Figure 9 shows plots of the positions of $-\overline{u'w'}$ and $\partial U/\partial z$ maxima within each of the downstream canopies. In the 06d patches (Fig. 9a–c), the $-\overline{u'w'}$ maxima remain within the canopy, whereas in the 14d patches (Fig. 9d–f), they are generally located above it, particularly in the weaker flows of the m14 and s14 cases. In all three 14d cases, the $-\overline{u'w'}$ maxima are decoupled from the $\partial U/\partial z$ maxima which are located within the canopy, implying that the Reynolds stress here is due to the decaying, advected turbulence rather than locally produced turbulence.

Figure 10 shows the spatial averages of $-\overline{u'}$ and $-\overline{w'}$, respectively, within the measurable portions of the canopies in all five patches from the fast-flow cases. The overall means of $-\overline{u'}$ and $-\overline{w'}$ are, respectively, 3.3 times and 4.2 times higher in the f06d patch than in the upstream patches, and 1.12 times and 1.22 times higher in the f14d patch than in the f06d patch. This is due to the downstream variation of TKE (not shown), which mimics that of $-\overline{u'w'}$ (Fig. 6). Since both patches reduce the TKE at approximately the same rate, the level of TKE within each patch is determined by its level at their upstream end. The TKE is higher at the upstream end of the f14d patch than it is at the upstream end of the f06d patch because it is closer to the position of the global Reynolds stress maximum.

Discussion

The results reported here suggest that patch–wake relationships are important in determining distributions of fauna

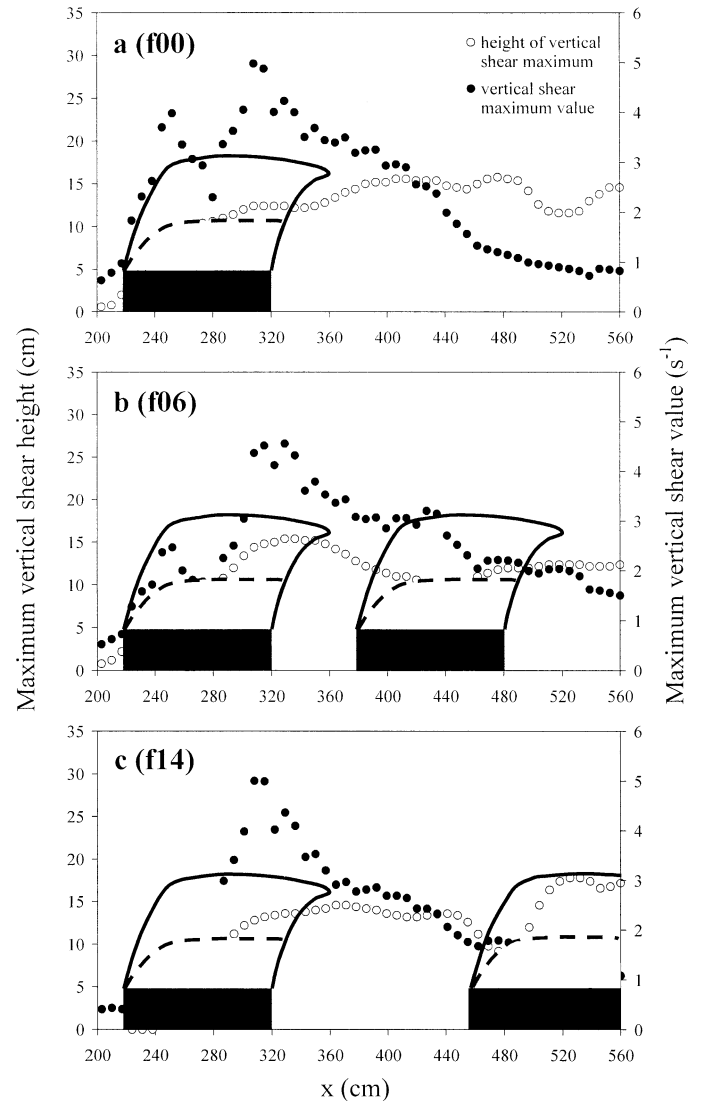


Fig. 8. Positions and values of the local vertical profile maxima of the vertical shear stress, $\partial U/\partial z$ for (a) the f00 case, (b) the f06 case, and (c) the f14 case. Data have been smoothed using a five-point rolling mean.

and nonmotile organisms. They imply that particles would remain in suspension longer in patches located within the wake of other patches than in those where patch spacing is greater than wake length. This would alter rates of pollen interception by seagrass carpels (Ackerman 2002) and would reduce the rates of deposition of bivalves and other pelagic larvae (Irlandi et al. 1999; Crimaldi et al. 2002). This implies that these “in-wake” patches would have sparser populations of adult bivalves and other fauna such as gastropods and polychaetes than homogeneous meadows (Bologna and Heck 2002). The high Reynolds stress values found in the wakes imply that organic (and mineral) particulates carried in them may readily be exchanged into the rapid overflow and thus have a greater likelihood of traveling beyond in-wake patches. This process would be exacerbated by the tendency for vertical turbulence to be stronger on the upper side of the wake (Fig. 5) and would cause further reduction

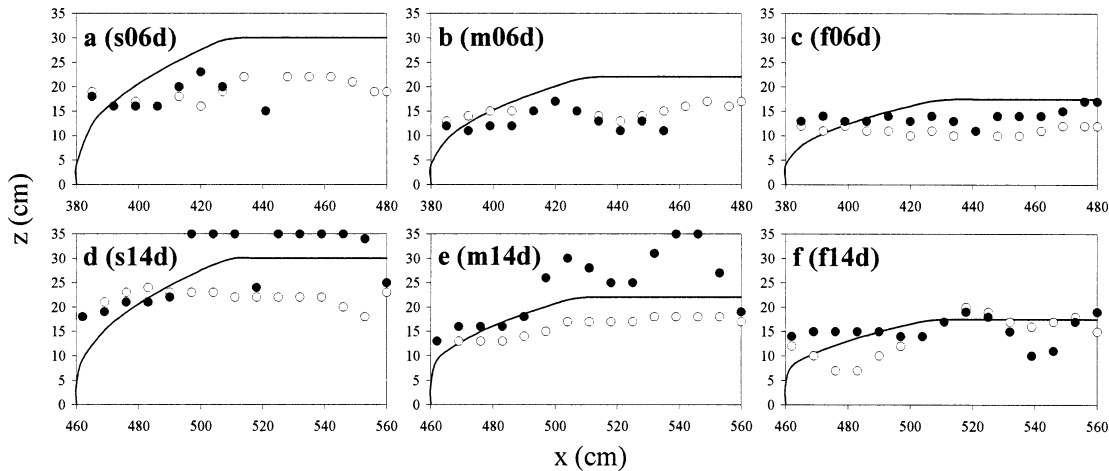


Fig. 9. Positions of the local vertical profile maxima of the Reynolds stress (filled circles) and vertical shear stress, $\partial U/\partial z$ (open circles) within or above the measurable portions of seagrass canopies for (a) f06d, (b) m06d, (c) s06d, (d) f14d, (e) m14d, and (f) s14d. The solid line in each plot indicates the top of the canopy. Data have been smoothed using a five-point rolling mean.

of the levels of larvae, pollen, etc., supplied to in-wake patches. Increased turbulence levels would increase the rate of supply of dissolved gases across the leaf-water interface, which would increase the rate of photosynthesis (Fonseca and Kenworthy 1987). However, they would also increase the retention of suspended particles in the canopy. This

would increase turbidity and thus attenuate the supply of light to the canopy. This in turn would reduce the rate of photosynthesis (Koehl and Alberte 1988). Which of these effects dominates would depend on local conditions (rate of sediment supply, depth of water, etc.) and thus it is not possible to say from these results whether the seagrass would benefit or suffer in this sense. Furthermore, because of the difficulties cited in taking measurements from the lower portions of the canopies, it is not possible to comment on changes in turbulence levels at the base of the patches or the changes in resuspension rates caused there.

The importance of seagrass patchiness in determining the distribution of fauna, passive organic particulates such as larvae and dissolved gases has long been noted. This research has found that patch size and isolation (e.g., Barbera-Cebrian et al. 2002; Hovel 2003), structural complexity in terms of shoot and biomass density (e.g., Irlandi 1997; Hovel 2003), and patch shape and orientation (Tanner 2003) are more important for determining faunal abundances and species richness than simply the areal extent of seagrass habitat. Patch edges have also been found to be particularly important in this respect: Faunal abundances have been found to be significantly higher at edge sites than in patch interiors or on bare substrate (e.g., Barbera-Cebrian et al. 2002; Bologna and Heck 2002). The present work shows, for the first time, the similar importance of patch-scale parameters (in particular patch isolation) on the hydrodynamics, thus providing a basis upon which ecohydrodynamic interactions at this scale can be investigated.

The key application of research in fragmented seagrass meadows lies in developing strategies for their recovery from natural and anthropogenic deterioration (as detailed by, for example, Short and Wyllie-Echeverria 1996). From this perspective, an understanding of the role hydrodynamics plays in determining “recoverability” is vital. The results presented are not able to provide immediately applicable insights. However, they do identify patch-wake relationships and thus patch spacing in relation to total wake length and the location of the wake Reynolds stress maximum as the

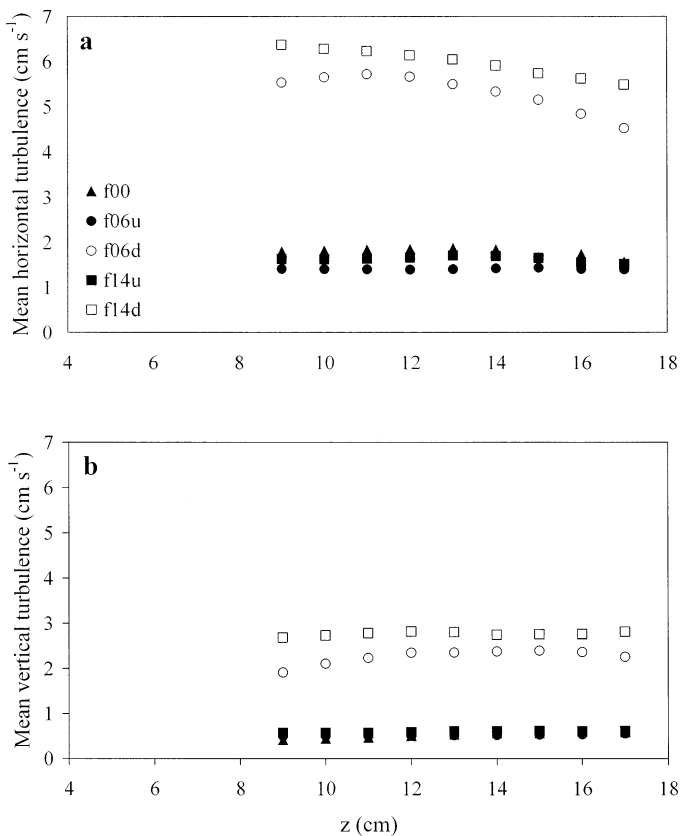


Fig. 10. Overall averages of (a) u' and (b) w' within the measurable portions of the canopies in all five patches from the fast-flow cases.

key hydrodynamic issue in this respect. Thus, they provide a platform from which further research on this topic can build. Specifically, they define three hydrodynamic states into which patchy meadows can be categorized. In the first, patch separation is greater than wake length, so that the patches are hydrodynamically isolated from each other. As patch separation decreases, a stage is reached of strong patch-wake interaction, with the ramifications discussed. Within this stage, patch location in relation to L_{NW} appears crucial. Finally, as the gaps between the patches get so small that there is insufficient space for wake evolution between them, the hydrodynamic characteristics of homogeneous meadows would prevail. These results also highlight differences in the effects of tidal and storm-driven currents. For the former, the different turbulence levels in the up- and downstream patches will be averaged out over each tidal cycle. However, these are relatively weak: The stronger, storm-driven currents will be more unidirectional and thus produce increased turbulence levels in downstream, in-wake patches, with the implications described above. As these changes will only occur during storm conditions, however, it is not clear how significant their overall impact may be.

This work has shown that to determine the hydraulic drag of patchy aquatic macrophyte distributions, there is a requirement to quantify the gap widths for which patches can be considered separate roughness elements and those for which they form indivisible patch-wake-patch elements. The threshold between these is determined by the total length of the upstream patch wake—the distance it takes for turbulence to return to levels found at the upstream end of the upstream patch. Only if the patches are separated by more than this distance can they be considered separate roughness elements. Otherwise, patch-wake-patch systems would need to be considered as compound roughness elements, the drag contribution of which would depend on the ratio of patch separation to L_{NW} .

There were a number of limitations to the experiments. Firstly, they simulated only conditions where the canopy height is at least 50% of the water depth, and not unconfined flow conditions where water depth is much greater than canopy height. Although the subcriticality of the flow noted above implies that in this sense they are qualitatively similar, the wake and flow separation phenomena observed, which are due in part to flow acceleration above the canopy, would be weaker in unconfined flows. Secondly, the ADV was unable to measure the lower half of the canopy, although flows in this region appeared uniformly very slow. Thirdly, the experiments were two-dimensional simplifications of natural flow patterns which are likely to be strongly three-dimensional. Thus these experiments should be viewed as a first step towards understanding their full complexity. Finally, the flows measured were nonuniform as they were developing from entrance conditions throughout the flume. However, the measurements indicate that any nonuniformities were small and swamped by the effects of the patches, which were our main interest.

The link identified here between the variation in wake turbulence intensity, patch separation and turbulence conditions in downstream patches implies that the last of these could be predicted by deriving a parameterization of the

wake-length scales (e.g., L_{NW} as defined above) in terms of easily measurable patch and flow parameters. Intuitively, one would expect these length scales to be a function of discharge rate, leaf length, flow depth, and patch separation. This work has shown that L_{NW} is inversely related to discharge rate (see, for example, Fig. 7) and quantified variations of turbulence intensity within wakes for specific values of flow rate, depth, and leaf length. These findings provide focus for the further work required to determine the full nature of these relationships. In nature, these relationships are likely to be complicated by the additional presence of wave action, which was not studied here and which dominates over mean flow in certain seagrass environments. Further work is required to gain understanding of the effect of waves on the flow-seagrass relationships found here. This is true not only of externally generated waves, but also of monami—large coherent waving motions apparently generated within seagrass canopies—which were not observed in these experiments as they have been in previous reports of flows in submerged vegetation (e.g., Ackerman and Okubo 1993). The currently accepted theory regarding their formation (e.g., Ghisalberti and Nepf 2002) states that they are caused by Kelvin-Helmholtz instability leading to large, coherent vortices within the shear layer at the top of the canopy. These vortices are advected downstream by the mean flow, causing the progressive, coherent waving of the vegetation. As such, their occurrence is partially determined by the flexibility of the canopy. Thus, the increased density of plants used here compared to previous studies in which they have been observed may increase the rigidity of the canopy to the point where they are suppressed. In addition, the relatively short length of seagrass patches used here, and the subsequent decay of the free shear layer, may not give the instabilities sufficient time to initiate and grow. Since Ghisalberti and Nepf's theory requires an extended free shear layer for the instabilities to grow, the lack of monami in these experiments can be seen as a corroboration of this theory.

In conclusion, these experiments have shown for the first time, albeit in an idealized configuration, the detailed structure of the hydrodynamic patterns within seagrass patches in a shallow-water environment. In particular, they have provided understanding of the nature of the turbulent wakes produced by patches and how this can affect conditions within other patches located in their path. They thus form a basis on which further research can be carried out in order to understand how these processes scale up to affect hydrodynamic, ecological, and sedimentary conditions at landscape scales and thus inform management of these important environments. This research will need to adapt the configurations used here so that they approximate natural conditions more closely—specifically they need to consider the three-dimensional character of natural patchy seagrass distributions and the added complexity of wave action in the hydrodynamic conditions—and relate findings from this type of controlled laboratory experimentation to direct measurements of natural seagrass meadows.

References

- ABDELRHMAN, M. A. 2003. Effect of eelgrass *Zostera marina* canopies on flow and transport. *Mar. Ecol. Prog. Ser.* **248**: 67–83.

- ACKERMAN, J. D. 2002. Diffusivity in a marine macrophyte bed: Implications for submarine pollination and dispersal. *Am. J. Bot.* **89**: 1119–1127.
- , AND A. OKUBO. 1993. Reduced mixing in a marine macrophyte canopy. *Funct. Ecol.* **7**: 305–309.
- BARBERA-CEBRIAN, C., P. SANCHEZ-JEREZ, AND A. A. RAMOS-ESPLA. 2002. Fragmented seagrass habitats on the Mediterranean coast, and distribution and abundance of mysids. *Mar. Biol.* **141**: 405–413.
- BOLOGNA, P. A. X., AND K. L. HECK. 2002. Impact of habitat edges on density and secondary production of seagrass-associated fauna. *Estuaries* **25**: 1033–1044.
- CORNELISEN, C. D., AND F. I. M. THOMAS. 2004. Ammonium and nitrate uptake by leaves of the seagrass *Thalassia testudinum*: Impact of hydrodynamic regime and epiphyte cover on uptake rates. *J. Mar. Syst.* **49**: 177–194.
- CRIMALDI, J. P., J. K. THOMPSON, J. H. ROSMAN, R. J. LOWE, AND J. R. KOSEFF. 2002. Hydrodynamics of larval settlement: The influence of turbulent stress events at potential recruitment sites. *Limnol. Oceanogr.* **47**: 1137–1151.
- DENNISON, W. C., AND R. S. ALBERTE. 1985. Role of daily light period in the depth distribution of *Zostera marina* (eelgrass). *Mar. Ecol. Prog. Ser.* **25**: 51–61.
- FONSECA, M. S., AND S. S. BELL. 1998. The influence of physical setting on seagrass landscapes near Beaufort, NC, USA. *Mar. Ecol. Prog. Ser.* **171**: 109–121.
- , AND J. S. FISHER. 1986. A comparison of canopy friction and sediment movement between four species of seagrass with reference to their ecology and restoration. *Mar. Ecol. Prog. Ser.* **29**: 15–22.
- , ———, J. C. ZIEMAN, AND G. W. THAYER. 1982. Influence of the seagrass *Zostera marina* L. on current flow. *Estuar. Coast. Shelf Sci.* **15**: 351–364.
- , AND W. J. KENWORTHY. 1987. Effects of current on photosynthesis and distribution of seagrasses. *Aquat. Bot.* **27**: 59–78.
- , J. C. ZIEMAN, G. W. THAYER, AND J. S. FISHER. 1983. The role of current velocity in structuring eelgrass (*Zostera marina* L.) meadows. *Estuar. Coast. Shelf Sci.* **17**: 367–380.
- GACIA, E., C. M. DUARTE, N. MARBA, J. TERRADOS, H. KENNEDY, M. D. FORTES, AND N. H. TRI. 2003. Sediment deposition and production in SE-Asia seagrass meadows. *Estuar. Coast. Shelf Sci.* **56**: 909–919.
- , T. C. GRANATA, AND C. M. DUARTE. 1999. An approach to measurement of particle flux and sediment retention within seagrass (*Posidonia oceanica*) meadows. *Aquat. Bot.* **65**: 255–268.
- GAMBI, M. C., A. R. M. NOWELL, AND P. A. JUMARS. 1990. Flume observations of flow dynamics in *Zostera marina* (eelgrass) beds. *Mar. Ecol. Prog. Ser.* **61**: 159–169.
- GHISALBERTI, M., AND H. M. NEPF. 2002. Mixing layers and coherent structures in vegetated aquatic flow. *J. Geophys. Res.* **107**: 1–11.
- GRANATA, T. C., T. SERRA, J. COLOMER, X. CASAMITJANA, C. M. DUARTE, AND E. GACIA. 2001. Flow and particle distributions in a nearshore seagrass meadow before and after a storm. *Mar. Ecol. Prog. Ser.* **218**: 95–106.
- HOVEL, K. A. 2003. Habitat fragmentation in marine landscapes: Relative effects of habitat cover and configuration on juvenile crab survival in California and North Carolina seagrass beds. *Biol. Conserv.* **110**: 401–412.
- IRLANDI, E. A. 1997. Seagrass patch size and survivorship of an infaunal bivalve. *Oikos* **78**: 511–518.
- , B. A. ORLANDO, AND W. G. AMBROSE. 1999. Influence of seagrass habitat patch size on growth and survival of juvenile bay scallops, *Argopecten irradians concentricus*. *J. Exp. Mar. Biol. Ecol.* **235**: 21–43.
- KAIMAL, J., AND J. FINNIGAN. 1994. Atmospheric boundary layer flows. Oxford Univ. Press.
- KELLY, N. M., M. S. FONSECA, AND P. E. WHITFIELD. 2001. Predictive mapping for management of seagrass beds. *Aquat. Cons. Mar. Freshw. Ecosyst.* **11**: 437–451.
- KOEHL, M. A. R., AND R. S. ALBERTE. 1988. Flow, flapping and photosynthesis of macroalgae: Functional consequences of undulate blade morphology. *Mar. Biol.* **99**: 435–444.
- LANE, S. N., AND OTHERS. 1998. Three-dimensional measurement of river channel flow processes using acoustic Doppler velocimetry. *Earth Surf. Proc. Landforms* **23**: 1247–1267.
- MADSEN, J. D., P. A. CHAMBERS, W. F. JAMES, E. W. KOCH, AND D. F. WESTLAKE. 2001. The interaction between water movement, sediment dynamics and submersed macrophytes. *Hydrobiologia* **444**: 71–84.
- MATEO, M. A., J. ROMERO, M. PEREZ, M. M. LITTLER, AND D. S. LITTLER. 1997. Dynamics of millenary organic deposits resulting from the growth of the Mediterranean seagrass *Posidonia oceanica*. *Estuar. Coast. Shelf Sci.* **44**: 103–110.
- MAZZELLA, L., M. C. BUIA, M. C. GAMBI, M. LORENTI, G. F. RUSSO, M. B. SCIPIONE, AND V. ZUPPO. 1995. A review on the trophic organisation in the *Posidonia oceanica* ecosystem, p. 40–47. *In* F. Cinelli, E. Fresi, C. Lorenzi, and A. Mucedola [eds.], *La Posidonia oceanica—un contributo per la salvaguardia del principale ecosistema marino del Mediterraneo*. Rivista Marittima.
- NEPF, H. M., J. A. SULLIVAN, AND R. A. ZAVISTOSKI. 1997. A model for diffusion within emergent vegetation. *Limnol. Oceanogr.* **42**: 1735–1745.
- , AND E. VIVONI. 2000. Flow structure in depth-limited vegetated flow. *J. Geophys. Res.* **105**: 28547–28557.
- PATTERSON, M. R., M. C. HARWELL, L. M. ORTH, AND R. J. ORTH. 2001. Biomechanical properties of the reproductive shoots of eelgrass. *Aquat. Bot.* **69**: 27–40.
- ROSE, C. D., AND C. J. DAWES. 1999. Effects of community structure on the seagrass *Thalassia testudinum*. *Mar. Ecol. Prog. Ser.* **184**: 83–95.
- SHORT, F. T., AND S. WYLLIE-ECHEVERRIA. 1996. Natural and human-induced disturbance of seagrass. *Environ. Conserv.* **23**: 17–27.
- TANNER, J. E. 2003. Patch shape and orientation influence on seagrass epifauna are mediated by dispersal abilities. *Oikos* **100**: 517–524.
- TEETER, A. M., B. H. JOHNSON, C. BERGER, G. STELLING, N. W. SCHEFFNER, M. H. GARCIA, AND T. M. PARCHURE. 2001. Hydrodynamic and sediment transport modeling with emphasis on shallow-water, vegetated areas (lakes, reservoirs, estuaries and lagoons). *Hydrobiologia* **444**: 1–24.

Received: 5 February 2004

Accepted: 16 March 2005

Amended: 21 April 2005